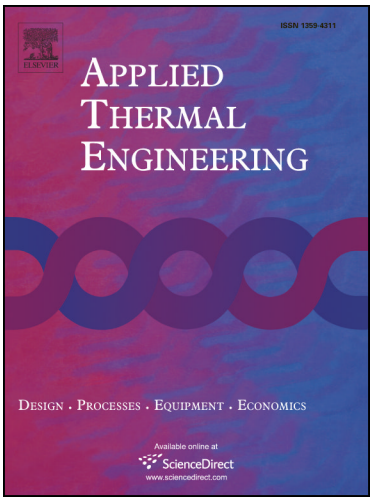

Optimization of thermal management system for Li-ion batteries using phase change material

Yantong Li, Yaxing Du, Tao Xu, Huijun Wu, Xiaoqing Zhou, Ziye Ling, Zhengguo Zhang

PII: S1359-4311(17)36609-7
DOI: https://doi.org/10.1016/j.applthermaleng.2017.12.055
Reference: ATE 11576

To appear in: *Applied Thermal Engineering*

Received Date: 15 October 2017
Revised Date: 21 November 2017
Accepted Date: 14 December 2017

Please cite this article as: Y. Li, Y. Du, T. Xu, H. Wu, X. Zhou, Z. Ling, Z. Zhang, Optimization of thermal management system for Li-ion batteries using phase change material, *Applied Thermal Engineering* (2017), doi: https://doi.org/10.1016/j.applthermaleng.2017.12.055

Optimization of thermal management system for Li-ion batteries using phase change material

Yantong Li[a], Yaxing Du[b], Tao Xu[c,*], Huijun Wu[c], Xiaoqing Zhou[c], Ziye Ling[d], Zhengguo Zhang[d]

[a] Department of Architecture and Civil Engineering, City University of Hong Kong, Tat Chee Avenue, Kowloon, Hong Kong
[b] Department of Building Services Engineering, The Hong Kong Polytechnic University, Hung Hom, Kowloon, Hong Kong
[c] School of Civil Engineering, Guangzhou University, Guangzhou 510006, China
[d] Key Laboratory of Enhanced Heat Transfer and Energy Conservation, The Ministry of Education, School of Chemistry and Chemical Engineering, South China University of Technology, Guangzhou 510640, China

*The corresponding author; Email: cetxu@scut.edu.cn

ABSTRACT

This study presents an optimization method of Li-ion battery thermal management system (BTMS) using phase change material (PCM). The optimization objective is to minimize the mass of PCM. Two design constraints should be satisfied during the optimization process: (1) the maximum temperature difference in the BTMS should not exceed the threshold value; (2) the desired working time of maintaining the batteries temperature under operation safe temperature should be fulfilled. A case study of the cylindrical BTMS with PCM is selected to illustrate the proposed optimization method. The expanded graphite (EG)/ paraffin (PA) composite PCM is used in the BTMS. The thermodynamic mathematical models of the system are solved by the commercial software computational fluid dynamics (CFD). The numerical results are validated against experimental data, and a good agreement has been achieved. During the optimization, four types of BTMS which respectively use single, double, three and four batteries, are considered. The effects of battery radius, gap between neighboring batteries, heat generation rate, and top and bottom PCM thickness on the minimum mass of PCM are analyzed. The optimal radiuses of the PCM unit in different conditions are identified. Results indicate that the proposed optimization method is effective

to optimize the BTMS with PCM, which provides guidelines for engineers to conduct the design optimization for similar systems.

Keywords: Optimization method; Li-ion battery; Battery thermal management system (BTMS); Phase change material (PCM)

Nomenclature

$cp_{battery}$	specific heat of the battery (kJ/kg·^{o}C)	T_{max}	transient maximum temperature (^{o}C)
cp_{PCM}	specific heat of PCM (kJ/kg·^{o}C)	T_{min}	transient minimum temperature (^{o}C)
H_{PCM}	enthalpy of PCM (kJ/kg)	$T_{num,ii}$	numerical temperature value (^{o}C)
h_{PCM}	sensible heat of PCM (kJ/kg)	T_{safe}	safe operation temperature (^{o}C)
ii	iteration number of the experimental sample (-)	T_0	initial temperature (^{o}C)
k_{PCM}	thermal conductivity of PCM (W/m·^{o}C)	t	time step (s)
$k_{battery}$	thermal conductivity of the battery (W/m·^{o}C)	$t_{desired}$	desired working time (s)
l_{BTMS}	length of BTMS (mm)	$t_{duration}$	duration time (s)
m_{PCM}	mass of PCM (kg)	x	space step in the *x* axis direction (m)
m_{min}	minimum mass of PCM	y	space step in the *y* axis direction (m)
$n_{battery}$	number of the batteries (-)	z	space step in the *z* axis direction (m)
nn	number of experimental sample (-)	δ_{ARE}	average relative error (%)
Q_{heater}	heat generation rate of the heater (kW)	δ_{BTMS}	top and bottom thickness of the BTMS (mm)
$Q_{battery}$	heat generation rate of the battery (kW)	β	liquid fraction (-)
$q_{battery}$	heat generation density of the battery (kW/m^3)	ρ_{PCM}	density of PCM (kg/m^3)
q_{heater}	heat generation density of the heater (kW/m^3)	$\rho_{battery}$	density of the battery (kg/m^3)
R_{PCM}	radius of PCM unit (mm)	φ	gap coefficient (-)
$R_{battery}$	radius of the battery (mm)	γ_{PCM}	specific latent heat of PCM (kJ/kg)
T_{PCM}	temperature of PCM (^{o}C)	ΔH_{PCM}	enthalpy change of PCM (kJ/kg)
		ΔR	distance between neighboring batteries (mm)
		ΔT_{max}	transient maximum temperature difference (^{o}C)

$T_{battery}$	temperature of the battery (^{o}C)	$\Delta T_{max,m}$	maximum temperature difference (^{o}C)
$T_{exp,ii}$	experimental temperature value (^{o}C)	$\Delta T_{permissible}$	permissible temperature difference (^{o}C)
T_m	phase change temperature of PCM (^{o}C)		

1. Introduction

As the rapid development of global industrialization increases, the increasing emission of the greenhouse gases and the energy crisis have become pressing issues for the society [1, 2]. To deal with the severe environmental and energy problems, pure/hybrid electric vehicles (EVs/HEVs) with green power system, which are more environmentally friendly than conventional vehicles with combustion engines [3, 4], are intensively designed and used. Li-ion batteries are selected as the most suitable power source for EVs/HEVs because of their high specific energy density, low weigh, low discharging rate, and good stability [5-7]. However, the applications of the Li-ion battery in the EVs/HEVs are often hindered by overheating problem, which results from untimely dissipation of generation heat [8, 9]. High operation temperature of the Li-ion battery will lead to safety problems and shorten the batteries lifespan [10], even the severe disasters such as fire and explosion [11, 12]. It was reported in the study of Jiang et al. [13] that the maximum battery operation temperature should not exceed 60^{o}C. Therefore, the development of BTMS is vital for Li-ion batteries because it can maintain battery operation temperature within suitable range.

Recently, lots of heat dissipation technologies have been proposed and studied in the BTMS to ensure the battery safety and expand the battery lifespan. One typical approach of cooling down the high-temperature Li-ion batteries is to use the cold air. For example, Saw et al. [14] designed a new BTMS with air cooling and conducted numerical investigation on its thermal performance. Park et al. [15] investigated the battery arrangements on the performance of the BTMS with air cooling. In the study of Mahamud et al. [16], the BTMS using reciprocating air cooling method was designed. However, this approach has some defects including the fan power which will deplete the batteries energy, and the low cooling efficiency [17]. Another typical heat dissipation technology used in the BTMS is the liquid cooling method. For example, Jarrett et al. [18, 19] conducted the design optimization of the BTMS with liquid cooling. Jin et al. [20] designed the ultra-thin mini-channel liquid cold plate for the batteries thermal management. The disadvantages of this approach are high investment cost, large space occupation and high power consumption [14], etc. Heat pipe is also regarded as one popular method which has been applied in the BTMS. For example, Wu et al. [21] proposed a

BTMS with heat pipe, which was inserted into an aluminum fin. Rao et al. [22] experimentally investigated the thermal performance of the BTMS with heat pipe. They reported that this method had a considerable energy saving potential when it was applied in the EVs/HEVs. Although the cooling efficiency of the BTMS with heat pipe is higher than the above two other methods, the system configuration is complex, and large energy supply is required to drive the heat pipe components [11].

In addition to the aforementioned methods, the utilization of PCM in the BTMS has become a thriving trend due to its prominent advantages: temperature stability, large latent heat, simple structure and low power consumption [23-25], etc. A variety of researches on the BTMS with PCM were conducted by the researchers [26-34]. For instance, Alshaer et al. [26, 27] numerically investigated the thermal performance of the BTMS with the composite PCM, which is made up of pure PCM, carbon foam and Nano carbon tubes. Huo et al. [28] used lattice Boltzmann method to solve the heat transfer mathematical models of the BTMS with PCM. The effect of the thermal conductivity and latent heat of the PCM on the system performance was analyzed. In the study of Liu et al. [29], the thermal behavior of the BTMS with PCM which consisted of twenty flat-plate batteries stacks was numerically investigated. Samimi et al. [30] numerically and experimentally conducted the thermal management performance analysis of the BTMS with PCM. The carbon fibers were added into the pure PCM to enhance its thermal conductivity to improve the system performance. In the study of Somasundaram et al. [31], the thermodynamic mathematical model for the BTMS with PCM, in which the shape of the Li-ion batteries was spiral, was derived and solved. Li et al. [32] designed a sandwiched BTMS with PCM, and experimentally analyzed its thermal management performance. The expanded graphite (EG)/ paraffin (PA) composite PCM was used in the BTMS designed by Lin et al. [33] to enhance the thermal conductivity of the pure PCM. Sasmito et al. [34] designed a BTMS with PCM, which could be used in the cold weather. However, the methods to conduct the optimization of BTMS with PCM were few reported in the previous studies. In order to establish the guideline for optimization of BTMS with PCM, a systematic and effective method is urgently needed.

In this study, a thermal performance optimization method for the BTMS with PCM is proposed. In order to illustrate this approach, the case study of a cylindrical BTMS is presented. The optimization objective is to minimize the mass of PCM, while ensuring that the desired working time and maximum temperature difference. CFD is used to solve the thermodynamic mathematical models. The experiment platform is constructed to prepare the EG/PA composite PCM, and the thermo-physical properties of PCM are used in the numerical optimization of the BTMS. Also, the experimental data is used to validate the reliability of the numerical simulation. During the optimization process, four types of BTMS with single, double, three, and four batteries are considered. The effects of the battery radius, the gap between the neighboring batteries, the battery heat generation, and top and bottom PCM thickness on the minimum mass of PCM are investigated. Meanwhile, the optimal PCM radiuses in different conditions are identified.

The rest of the paper is organized as follows. Section 2 describes the proposed method for the optimization of BTMS with PCM. Section 3 introduces the case study that is used to illustrate the optimization method. The experimental section is shown in the Section 4. Section 5 presents the result analysis and relevant discussions. Concluding remarks are given in Section 6.

2. Methodology

In this study, the optimization objective is to minimize the mass of PCM (m_{PCM}). The mass of PCM is usually regarded as an important evaluation index in the energy storage system [35, 36], because the amount of PCM mass is related to the initial investment cost of BTMS. Noted that during the optimization procedure, two design constraints should be satisfied: (1) the desired working time ($t_{desired}$) of maintaining the Li-ion batteries temperature ($T_{battery}$) under the safe operation temperature (T_{safe}) should be satisfied; (2) the maximum temperature difference ($\Delta T_{max,m}$) in the BTMS should not exceed the permissible

temperature difference value ($\Delta T_{permissible}$). It should be mentioned that $\Delta T_{max,m}$ is the maximum value of the difference between the transient maximum and minimum temperature in the BTMS during the desired operation period, which is determined as Eq. (1). The first design constraint is set since the duration time ($t_{duration}$) of maintaining the $T_{battery}$ under the T_{safe} is one of the fundamental requirements in BTMS [8, 17]. Besides, certain amount of working time ($t_{desired}$) must be assured in BTMS. Thus, in the optimization procedure the $t_{duration}$ should be greater than $t_{desired}$. The second design constrain is set because large temperature difference in BTMS will accelerate their ageing and reduce their lifetime [11, 13]. Therefore, the ΔT_{max} should not exceed the $\Delta T_{permissible}$.

$$\Delta T_{max,m} = \max\{T_{max}(t) - T_{min}(t)\}, \quad t \le t_{desired} \tag{1}$$

where T_{max} and T_{min} are the transient maximum and minimum temperature, respectively.

The description of the optimization procedure is shown in Fig. 1. Firstly, the initial geometry of the BTMS with PCM should be identified before the optimization. Then the heat transfer process of the BTMS is solved in the CFD software. Meanwhile, the $t_{duration}$ and ΔT_{max} are recorded after completing the calculation. If $\Delta T_{max,m}$ is less than $\Delta T_{permissible}$ and $t_{duration}$ is larger than $t_{desired}$, it will go to the next step. Otherwise, the geometry of the BTMS will be changed, and then new round of calculation will be performed. For the next step, it will judge whether the m_{PCM} in the current case is minimum. If m_{PCM} is the minimum, the optimal geometry parameters of the BTMS will be acquired. Otherwise, the new round of calculation will be performed until the optimization is completed.

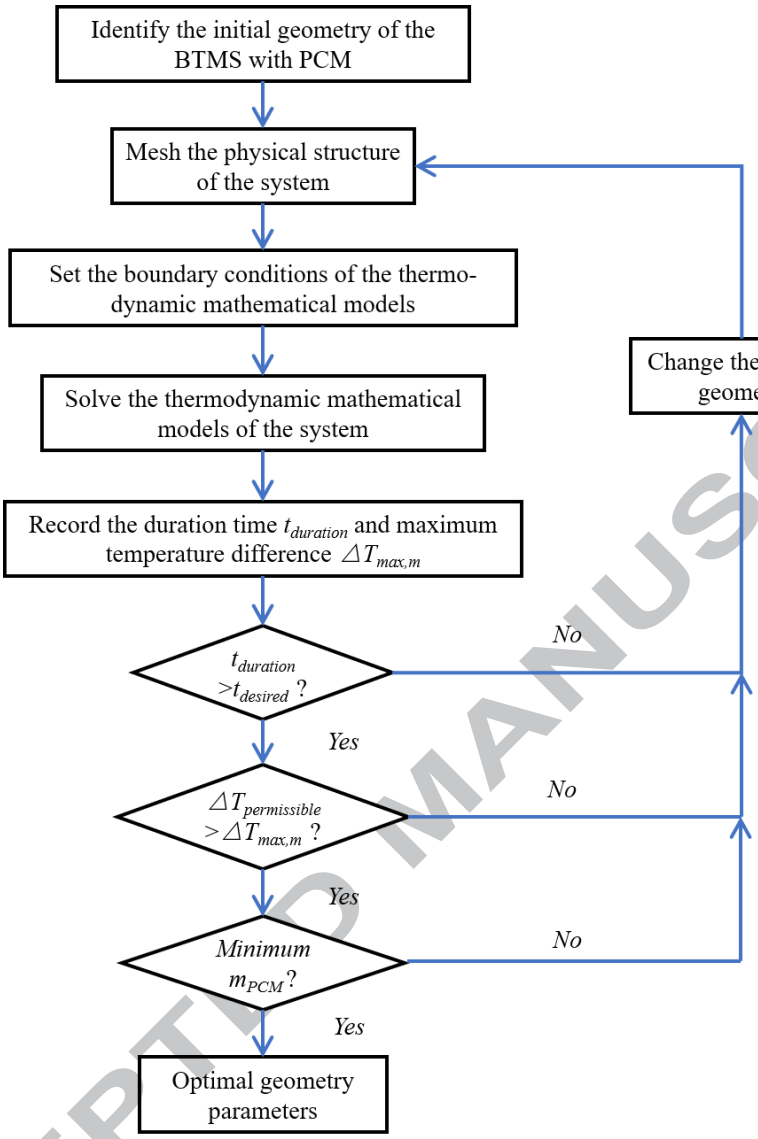

Fig. 1. Optimization procedure for the BTMS with PCM.

3. Case study

3.1 Cylindrical BTMS with PCM

The schematic diagram of the cylindrical BTMS with PCM is shown in Fig. 2. The shape of Li-ion batteries and PCM unit are cylindrical [5, 37]. Li-ion batteries are symmetrically inserted into the PCM unit, which is used to maintain the battery temperature within the safe operation range. The heat generated by the Li-ion batteries will be transferred to the PCM unit, and thus the hot Li-ion batteries are cooled down. When the temperature of the PCM unit reaches the phase change temperature, the solid PCM will gradually melt. During the

phase change process, the rising trend of Li-ion battery temperature will slow down because of the isothermal characteristic of the PCM. Besides, the large latent heat of the PCM further helps to improve the cooling effect of the BTMS. Thus, the working life and the safety of Li-ion batteries can be well enhanced when the BTMS with PCM is applied. It should be mentioned that the thermal insulation layer is used outside the PCM unit, which can prevent the heat exchange between the BTMS and surrounding environment.

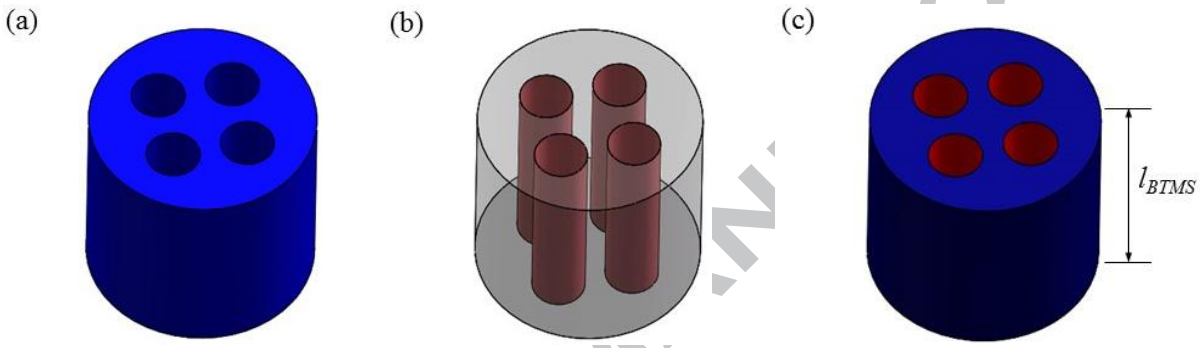

Fig. 2. The schematic diagram of the BTMS: (a) PCM filled closed unit; (b) Li-ion batteries; (c) BTMS with PCM.

3.2 Numerical study

3.2.1 Mathematical models

The mathematical models of the BTMS are made up of two parts: PCM unit and Li-ion batteries. The enthalpy method, which is one of the commonly used numerical methods [34], is used to solve the heat transfer process of the PCM unit in this study. In order to simplify the numerical simulation, several assumptions are proposed as following: (i) the thermo-physical properties of the PCM are constant; (ii) the radiation is not considered in the calculation process; (iii) the exterior surface of the PCM unit is thermally insulated; (iv) the viscosity of the PCM is regarded as 1×10^5 $\mathrm{kg/(m\cdot s)}$ because no liquid motion exists in the PCM unit.

Based on the above assumptions, the energy conservation equation of the PCM model can be expressed as the following equations:

$$\rho_{PCM}\frac{\partial H_{PCM}}{\partial t} = k_{PCM}\left(\frac{\partial^2 T_{PCM}}{\partial x^2} + \frac{\partial^2 T_{PCM}}{\partial y^2} + \frac{\partial^2 T_{PCM}}{\partial z^2}\right) \quad (2)$$

where ρ_{PCM} is the density of the PCM; H_{PCM} is the enthalpy of the PCM; t is the time step, k_{PCM} is the thermal conductivity of the PCM; and T_{PCM} is the temperature of the PCM. x, y, and z are the space step in these three different directions.

$$H_{PCM} = h_{PCM} + \Delta H_{PCM} \tag{3}$$

where h_{PCM} is the sensible heat of the PCM; and ΔH_{PCM} is the enthalpy change during the phase change process.

$$h_{PCM} = \int_{T_0}^{T_{PCM}} cp_{PCM}\, dT_{PCM} \tag{4}$$

where T_0 is the initial temperature, which is 25°C in this study. cp_{PCM} is the specific heat of the PCM.

$$\Delta H_{PCM} = \beta \gamma_{PCM} \tag{5}$$

where γ_{PCM} is the specific latent heat of the PCM. β is the liquid fraction of the PCM, which is expressed as the following equation:

$$\beta = \begin{cases} 0 & T_{PCM} < T_m \\ 1 & T_{PCM} > T_m \end{cases} \tag{6}$$

The energy conservation equation of the Li-ion batteries model can be expressed as the following equation:

$$\rho_{battery} cp_{battery} \frac{\partial T_{battery}}{\partial t} = k_{battery} \left(\frac{\partial^2 T_{battery}}{\partial x^2} + \frac{\partial^2 T_{battery}}{\partial y^2} + \frac{\partial^2 T_{battery}}{\partial z^2} \right) + q_{battery} \tag{7}$$

where $\rho_{battery}$ is the density of the battery; $cp_{battery}$ is the specific heat of the battery; $T_{battery}$ is the temperature of the battery; $k_{battery}$ is the thermal conductivity of the battery; and $q_{battery}$ is the heat generation flow rate per unit volume.

3.2.2 Initial and boundary conditions

The initial condition:

$$T_{PCM}(x, y, z) = T_{battery}(x, y, z) = T_0, \; t = 0 \tag{8}$$

The boundary condition of the contact surface between the batteries and PCM unit:

$$-k_{battery} \frac{\partial T_{battery}}{\partial n} = -k_{PCM} \frac{\partial T_{PCM}}{\partial n} \tag{9}$$

The boundary condition of the contact surface between the PCM unit and the surrounding environment:

$$-k_{PCM} \frac{\partial T_{PCM}}{\partial n} = 0 \tag{10}$$

3.2.3 Numerical solution

The finite element method (FEM) is used to solve the governing equations of the thermodynamic mathematical models. The mesh of the BTMS physical structure is constructed by the ICEM [38]. The commercial CFD software FLUENT [39] is used to simulate the heat transfer process between the PCM unit and Li-ion batteries. Fig. 3 shows the grid independency of the BTMS with PCM. The surface temperature variations of Li-ion batteries with three different grid numbers are presented. The temperature value with the minimum grid size of 2mm is very close to that with the minimum grid size of 5mm. The temperature value with the minimum grid size of 10mm is evidently different with other mesh systems. Thus, considering the simulation accuracy and computational cost the minimum grid size of 5mm is selected. Besides, the time steps of 1s, 0.5s, and 0.2s have been tested during the calculation process. It is found that there is almost no difference between the numerical results at these different time steps. Therefore, 1s is selected as the time step in our numerical simulation for saving the computational cost. In the solution methods panel the second-order upwind difference scheme is set for energy, and the first order implicit is set for transient formulation. The other parameters regarding the flow motion in both the solution methods and solution controls are set as default. The residual value for energy equation is set to 1e-8.

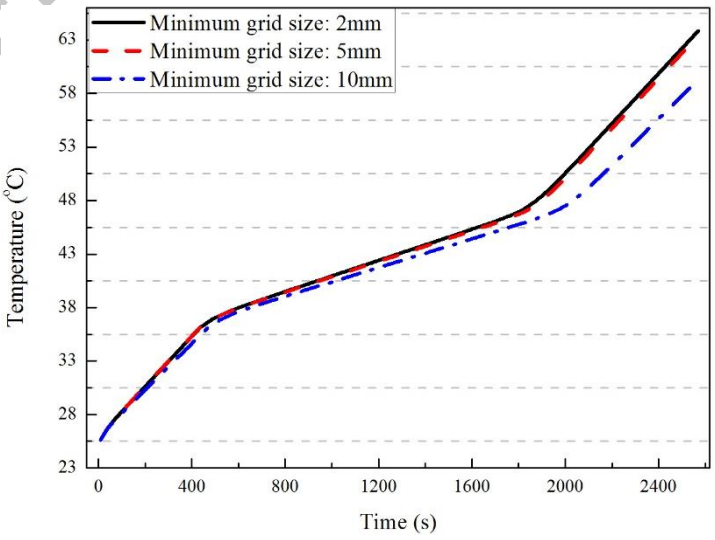

Fig. 3. Grid independency of the BTMS with PCM.

3.3 Identification of optimization index

The $\Delta T_{permissible}$ is set to be 5°C, as refers to [40]. The T_{safe} in the optimization is set to be 60°C, which refers to the previous studies in the [13, 40, 41]. The $t_{desired}$ is assumed to be 3000s in this case study. The m_{PCM} in this study can be expressed as the following equations:

$$m_{PCM} = \rho_{PCM} l_{BTMS} (\pi R_{PCM}^2 - n_{battery} \pi R_{battery}^2) \quad (11)$$

where l_{BTMS} is the length of the BTMS, which is assumed to be 100mm [37]. R_{PCM} is the radius of the PCM unit; $R_{battery}$ is the radius of the Li-ion batteries; and $n_{battery}$ is the number of the batteries in the BTMS. Four different types of BTMS which respectively include single battery, two batteries, three batteries and four batteries are considered in this study, as shown in Fig. 4. ΔR is the distance between the center of two neighboring batteries. The gap coefficient φ is defined as the ratio between ΔR and $R_{battery}$, which can be calculated as the following equation:

$$\varphi = \frac{\Delta R}{R_{battery}} \quad (12)$$

It should be noticed that in the BTMS with single battery the center of the PCM unit coincides with the center of the battery, which means that $\Delta R = 0$.

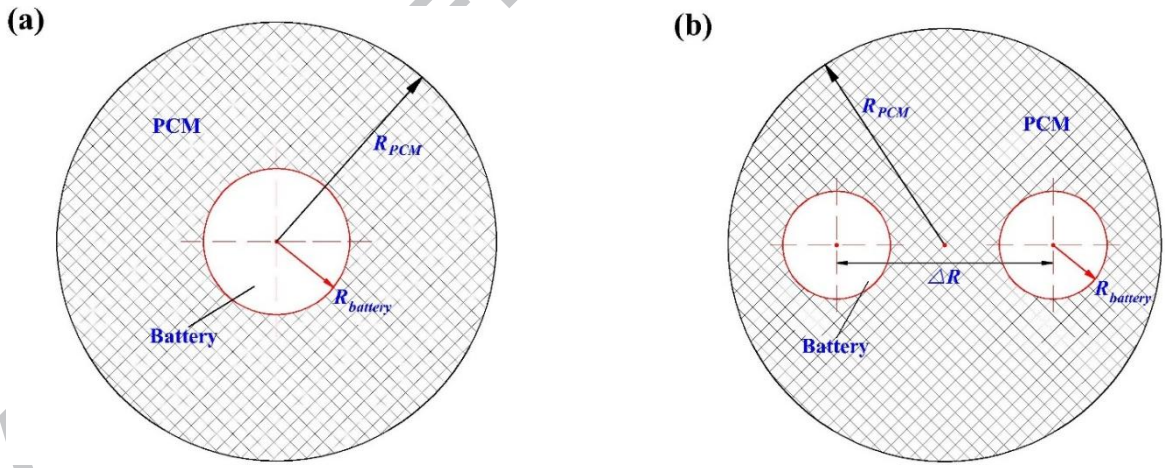

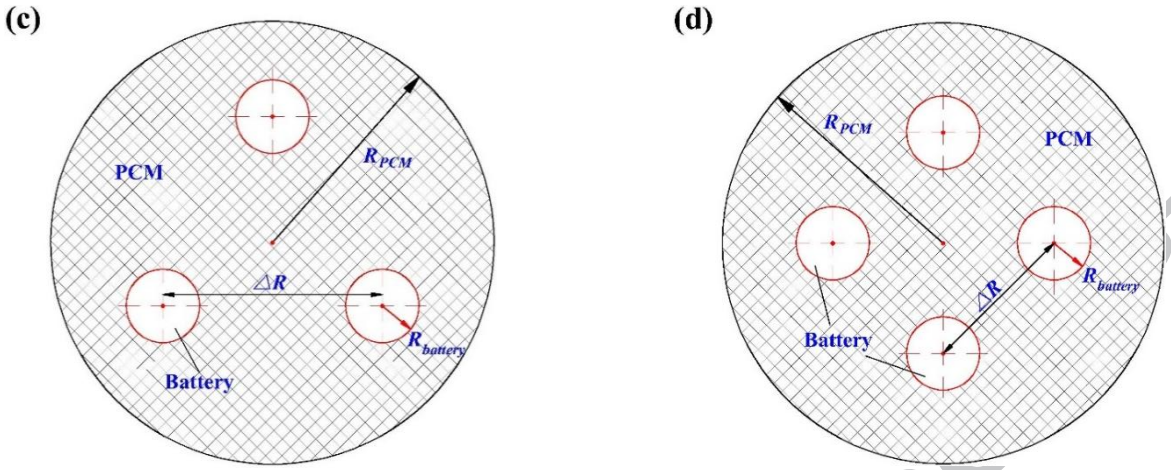

Fig. 4. Four different types of BTMS: (a) single battery; (b) two batteries; (c) three batteries; (d) four batteries.

4. Experimental study

4.1 Preparation of the EG/ PA composite PCM

As a commonly used PCM, PA is widely used in energy storage systems. However, the low thermal conductivity of the pure PA restricts its application because of the fact that this will result in the low heat transfer rate [42]. Therefore, during the recent years researchers proposed the method of using the EG to enhance the thermal conductivity of the PCM [37, 43]. In this study, the EG/PA composite PCM, which was prepared by adding the EG with the mass ratio of 25% into the PA (RT44HC), was applied in the BTMS. The detailed preparation process is presented as follows. Firstly, the micro-wave oven with the power of 900 W was used to heat the graphite to acquire the EG. Secondly, the PA was put into the beaker, which was placed inside the dryer with 60^{o}C to ensure the PA melt completely. Thirdly, the EG was added into the PA, and then the composites were fully mixed. Finally, the beaker was taken out from the dryer. After cooling down, the EG/PA composite PCM was obtained. The differential scanning calorimeter (DSC, Q20, America, TA Instruments Inc) was used to measure the phase change enthalpy and specific heat capacity of the composite PCM. The thermal constants analyzer (TPS 2500, Sweden, Hotdisk Inc) was utilized to measure the thermal conductivity of the composite. Table 1 shows the thermo-physical properties of the EG/PA composite PCM.

Table 1 The thermo-physical properties of the EG/PA composite PCM

Property	Value
Melting temperature (℃)	44
Latent heat (J/kg)	87900
Specific heat (J/(kg · ℃))	2500
Density (kg/m^3)	890
Thermal conductivity (W/(m · ℃))	10.8

4.2 Establishment of test rig

The aim of conducting the experiment is for the validation of the numerical mathematical models. Fig. 5 shows the schematic diagram of the test rig for the BTMS with PCM. The test rig consists of voltage output operation box, data logger (Agilent 34970A), computer, K-type thermocouples and tested BTMS, etc. The tested BTMS is made up of four electrical heaters and EG/PA composite PCM unit. The electrical heaters with a radius of 9mm and a length of 100mm, which are used for simulating Li-ion batteries, are placed axisymmetrically in the stainless-steel cylinder. The cylinder with a radius of 54mm and a length of 100mm, has a thermal insulation layer outside to prevent the heat exchange between the PCM and the surrounding environment. Two K-type thermocouples are respectively arranged at the Location #1 and Location #2 to measure the temperature values of the responding locations. The measurement accuracy of temperature values in each location is ±1^{o}C. The data logger is used to collect and record the data tested from the thermocouples. The computer that links with the data logger is utilized to handle and save the recorded data. It is also used to control the output of the voltage output operation box by transferring the signal. The voltage output operation box is used to provide heat for the electrical heaters in three different heat generation rate 5 W, 10 W, and 15 W. The heat generation rate can be controlled by the output voltage from the voltage output operation box, which can be calculated by the following equation:

$$Q_{heater} = \frac{U_{heater}^2}{R_{heater}} \tag{13}$$

where Q_{heater} is the heat generation rate of the electrical heater; U_{heater} and R_{heater} are the voltage and electric resistance of the electrical heater, respectively. The measurement accuracy of voltage and electric resistance values for each electrical heater are ±1V and ±1Ω, respectively. The according heat flow density are respectively 196,487 W/m^3, 392,975 W/m^3,

and 589,463 W/m^3, which can be calculated from the following equation:

$$q_{heater} = \frac{Q_{heater}}{V_{heater}} \tag{14}$$

where q_{heater} and V_{heater} are the heat flow density and volume of the electrical heater, respectively.

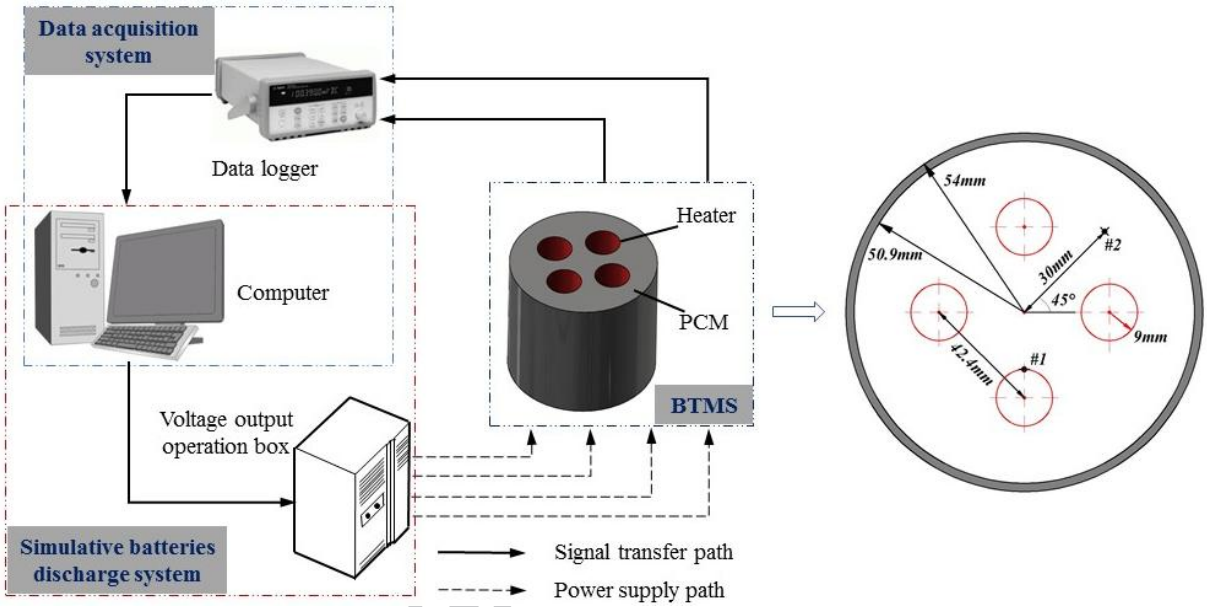

Fig. 5. The schematic diagram of the test rig for the BTMS with PCM.

5. Results and discussion

5.1 Model validation

In order to validate the accuracy of the mathematical models, the comparison between the experimental and numerical results is presented in the Fig. 6. It can be seen that the differences between the numerical and experimental temperature values are subtle. To be able to quantitatively assess the numerical accuracy, the average relative error (δ_{ARE}), which is calculated by the Eq. (15), is utilized here. The results of δ_{ARE} in different heat generation rate is presented in Table 2. The maximum and minimum δ_{ARE} is 4.86% and 1.30%, which suggests that there is a good agreement between the numerical and experimental results. Therefore, the mathematical models applied in the numerical calculation process are reliable and accurate.

$$\delta_{ARE} = \frac{1}{nn}\sum_{ii=1}^{ii=nn}\left|\frac{T_{exp,ii}-T_{num,ii}}{T_{exp,ii}}\right| \times 100\% \tag{15}$$

where nn is the number of experimental sample. $T_{exp,ii}$ and $T_{num,ii}$ are the experimental and

numerical temperature values, respectively.

Table 2 The average relative errors in different heat generation rate

	5kW	10kW	15kW
Location #1	2.81%	1.91%	4.86%
Location #2	2.90%	1.30%	1.81%

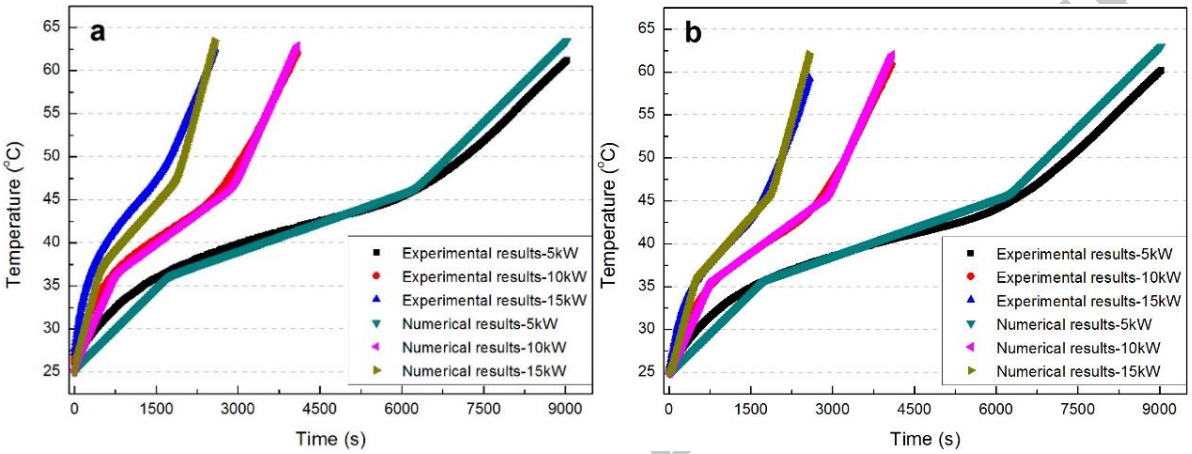

Fig. 6. The comparison between the numerical and experimental results : (a) #1; (b) #2.

5.2 Effect of battery radius

In order to illustrate how to identify the minimum PCM radius (R_{PCM}), a case study of Type III of BTMS is firstly presented in this section. The battery radius $R_{battery}$ and the gap coefficient φ are set to be 13mm and 2.2, respectively. The heat generation rate ($Q_{battery}$) is set to be 15W. Fig. 7 shows the variation of the maximum temperature difference with time for different PCM radius. The ΔT_{max} value increases with the increase of the PCM radius. The maximum value of the ΔT_{max} is nearly 2.9°C when the PCM radius is 48mm. Similarly, the maximum value of the ΔT_{max} is nearly 3.5°C when the PCM radius is 55mm. Thus, the values of the ΔT_{max} for all different PCM radius are less than 5°C, which satisfies the first design constraint. Fig. 8 shows the variation of the battery temperature for different PCM radius. It can be obtained that the ascending tends of these typical curves are almost same; the ascending degree is firstly sharp, then slow and sharp again at the end. The slow ascending trend results from the phase change process of the PCM, which has stable temperature. The value of $t_{duration}$ increases with the increase of the PCM radius. The values of $t_{duration}$ are respectively 2726s, 2855s, 2984s, 3010s, 3116s, 3184s and 3388s when the corresponding PCM radiuses are respectively 48mm, 49mm, 50mm, 50.2mm, 51mm, 51.5mm, and 52mm.

Therefore, the constraint of $t_{duration}$ can be fulfilled when the PCM radiuses are 50.2mm, 51mm, 51.5mm, 52mm, and 54mm. It is obvious that 50.2mm is the minimum PCM radius. According to the Eq. (11), the minimum mass of PCM (m_{min}) results from the case in which PCM radius is the minimum value. Thus, the value of m_{min} in this case study is equal to 0.5626kg.

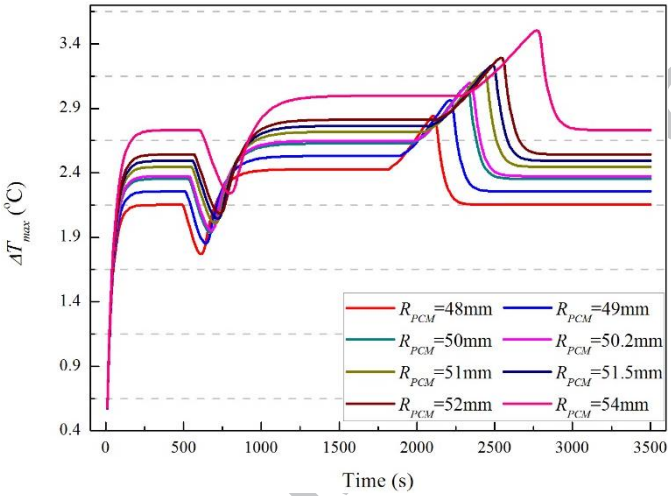

Fig. 7. The variation of the maximum temperature difference with time for different PCM radius.

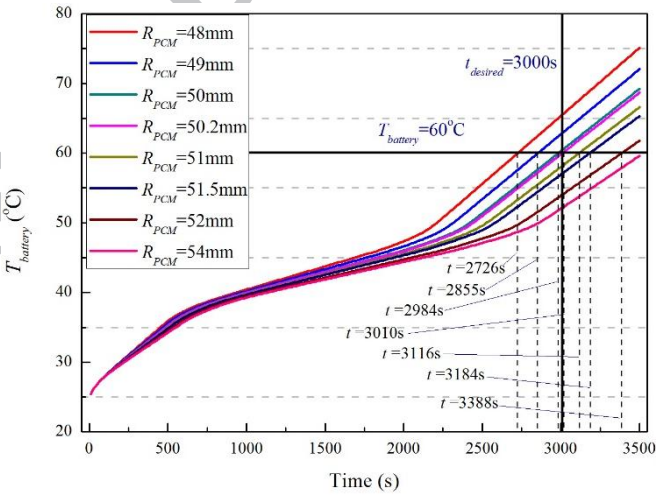

Fig. 8. The variation of the battery temperature with time for different PCM radius.

Fig. 9 shows the variation of m_{min} with the battery radius ($R_{battery}$) for four different BTMS types. It can be seen that the m_{min} decreases with the increase of the $R_{battery}$. This is because the heat density flow rate ($q_{battery}$) reduces when the $R_{battery}$ increases. For Type I, Type II, Type III, and Type IV of BTMS, the m_{min} is respectively decreased by 16.3%, 15.6%, 11.6%, and 14.8%, as the $R_{battery}$ varies from 3mm to 13mm.

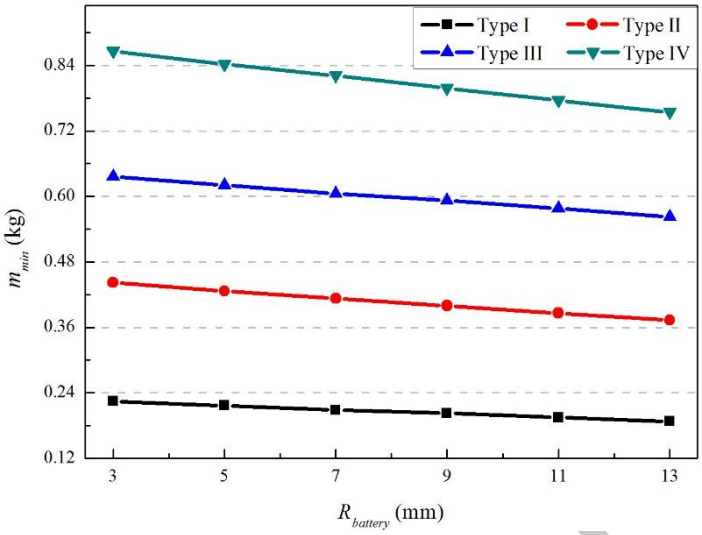

Fig. 9. The variation of the m_{min} with the battery radius for four different types of BTMS.

5.3 Effect of gap between neighboring batteries

To be able to illustrate the effect of the gap between neighboring batteries (ΔR) on the minimum PCM radius (R_{PCM}), the case study of three different ΔR values is firstly presented here. It should be noted that Type IV of BTMS is studied, and the $R_{battery}$ is set to be 13mm. Fig. 10 shows the variation of the maximum temperature difference with time for these three different cases: (a) $\Delta R = 2.4R_{battery}$; (b) $\Delta R = 2.6R_{battery}$; (c) $\Delta R = 2.8R_{battery}$. The value of the ΔT_{max} increases with the increase of the R_{PCM} in these three cases. It can be seen that in Fig. 10(a) the maximum ΔT_{max} is 3.8°C; in Fig. 10(b) the maximum ΔT_{max} is 3.3°C; and in Fig. 10(c) the maximum ΔT_{max} is 2.9°C. Thus, the values of the ΔT_{max} are all less than 5°C when R_{PCM} varies from 55mm to 61mm, which suggests that the first design constraint is satisfied in these cases.

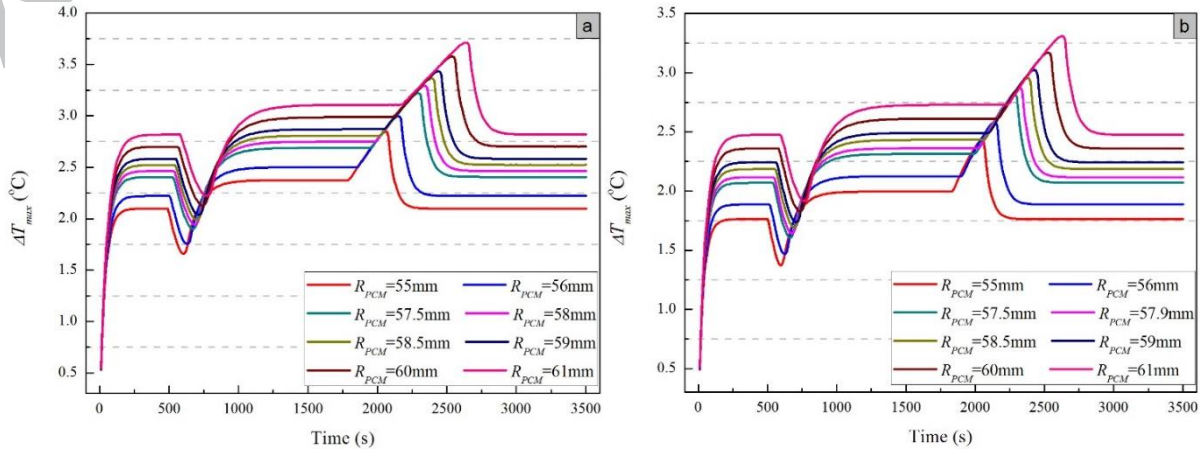

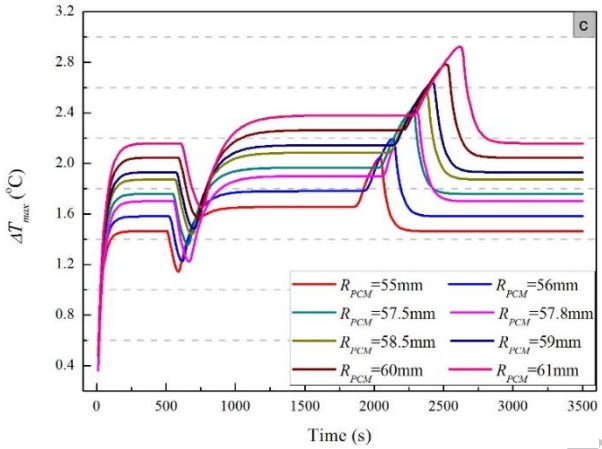

Fig. 10. The variation of the maximum temperature difference variation with time for three different cases: (a) $\Delta R = 2.4R_{battery}$; (b) $\Delta R = 2.6R_{battery}$; (c) $\Delta R = 2.8R_{battery}$.

Fig. 11 shows the variation of the battery temperature with the time for three different cases: (a) $\Delta R = 2.4R_{battery}$; (b) $\Delta R = 2.6R_{battery}$; (c) $\Delta R = 2.8R_{battery}$. It can be seen that the variation trends of Li-ion battery temperature ($T_{battery}$) for different ΔR values are similar. Besides, for a given time the larger R_{PCM} values have lower $T_{battery}$ values among these different R_{PCM} values. Moreover, the $t_{duration}$ increases with the increase of the R_{PCM}. In Fig. 11(a), the value of $t_{duration}$ is 2678s when the R_{PCM} value is 55mm; and the value of $t_{duration}$ is 3356s when the R_{PCM} value is 61mm. In Fig. 11(b), the value of $t_{duration}$ is 2688s when the R_{PCM} value is 55mm; and the value of $t_{duration}$ is 3370s when the R_{PCM} value is 61mm. In Fig. 11(c), the value of $t_{duration}$ is 2696s when the R_{PCM} value is 55mm; and the value of $t_{duration}$ is 3382s when the R_{PCM} value is 61mm. To satisfy the second design constrain ($t_{duration} > t_{desired}$), the minimum values of R_{PCM} are 58.0mm, 57.9mm, and 57.8mm for the responding ΔR values of $2.4R_{battery}$, $2.6R_{battery}$, and $2.8R_{battery}$, respectively. Thus, the values of m_{min} in these three cases are equal to 0.7512kg, 0.7480kg, and 0.7447kg, respectively.

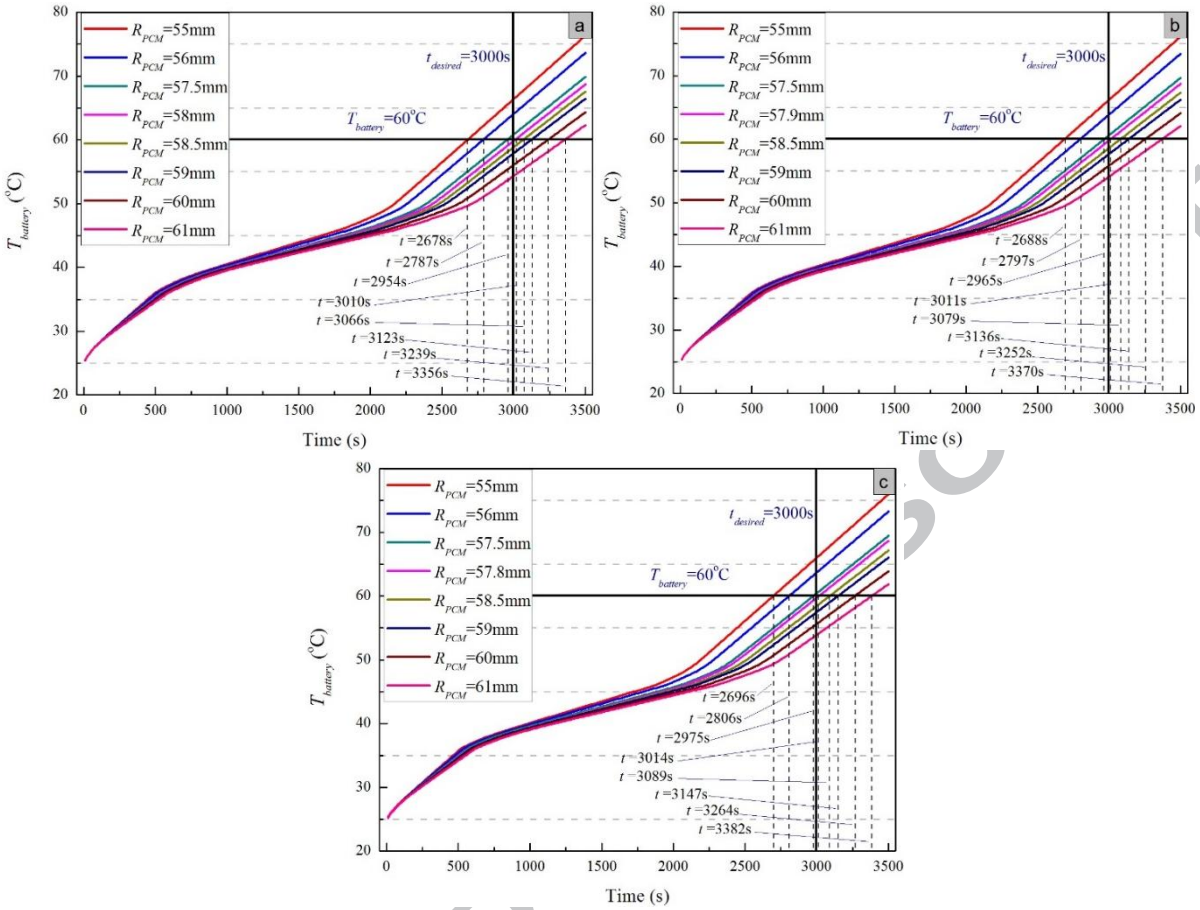

Fig. 11. The variation of the battery temperature variation with the time for three different cases: (a) $\Delta R = 2.4R_{battery}$; (b) $\Delta R = 2.6R_{battery}$; (c) $\Delta R = 2.8R_{battery}$.

Fig. 12 shows the effect of the gap coefficient (φ) on the m_{min} for three different types of BTMS: (a) Type II; (b) Type III; and (c) Type IV. Noted that for Type I of BTMS, the value of φ is 0. It can be observed that the value of m_{min} firstly reduces when the value of φ increases, and then it increases with the increase of φ value. Therefore, the optimal values of φ are 2.6, 3.4 and 3.4 for Type II, Type III, and Type IV of BTMS, respectively. In addition, the minimum values of m_{min} are 0.3685kg, 0.5514kg, and 0.7351kg for Type II, III, and IV of BTMS, respectively.

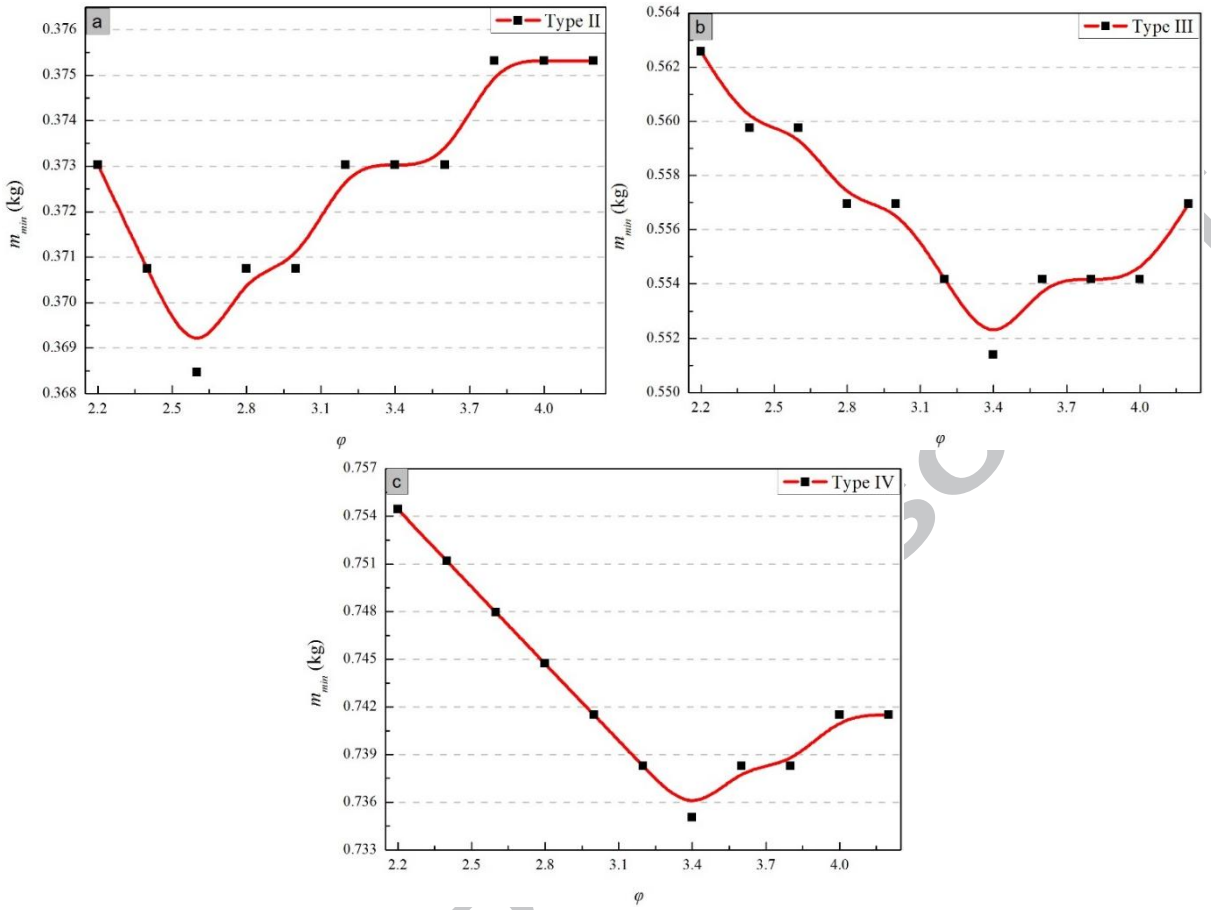

Fig. 12. The variation of m_{min} with φ in different type BTMS: (a) Type II; (b) Type III; and (c) Type IV.

5.4 Effect of heat generation rate

Fig. 13 shows the variation of ΔT_{max} with time for different heat generation rate ($Q_{battery}$). In this part, Type IV of BTMS is selected as the research object. The values of $R_{battery}$ and φ are set as 13mm and 3.4, respectively. The transient maximum ΔT_{max} value increases with the increase of $Q_{battery}$ values. The maximum ΔT_{max} value is nearly 4.3°C when the $Q_{battery}$ value is equal to 23W; and the maximum ΔT_{max} value is approximately 2.8°C when the $Q_{battery}$ value is equal to 15W. Thus, if the value of $Q_{battery}$ is too large, the maximum ΔT_{max} value in the BTMS will exceed 5°C, which fails to satisfy the first design constrain.

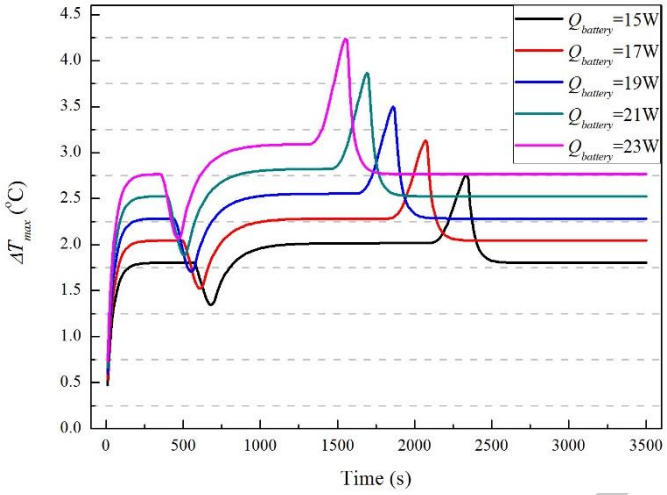

Fig. 13. The variation of ΔT_{max} with time for different $Q_{battery}$.

Fig. 14 shows the variation of $T_{battery}$ with time for different $Q_{battery}$. It can be seen that the value of $T_{battery}$ tends to be higher when the $Q_{battery}$ value is larger. This phenomenon can be explained by the fact that the value of the heat density flow ($q_{battery}$) is higher when the $Q_{battery}$ value is larger according to the Eq. (13). Besides, the duration time ($t_{duration}$) decreases with the increase of $Q_{battery}$ values. When $Q_{battery}$ value increases from 15W to 23W, the $t_{duration}$ value varies from 3001s to 1941s, reduced by 35.3%. Therefore, it means that more amount of PCM mass is required to maintain the desired time ($t_{desired}$) as the value of $Q_{battery}$ increases.

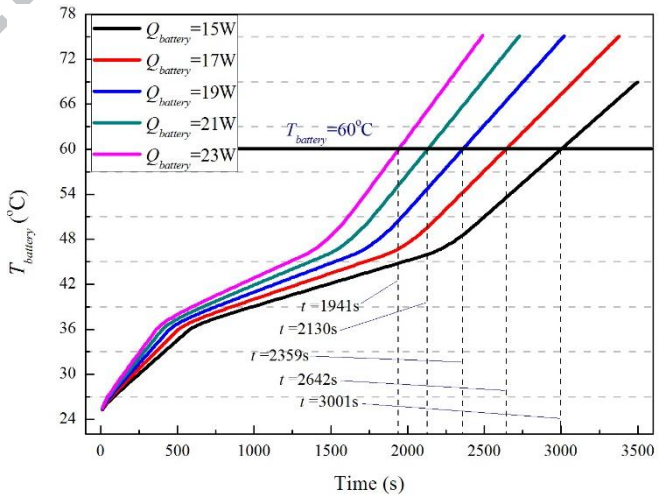

Fig. 14. The variation of $T_{battery}$ with time for different $Q_{battery}$.

Fig. 15 shows the variation of the minimum mass of PCM (m_{min}) with the $Q_{battery}$ for

different types of BTMS. It can be obtained that the value of m_{min} increases with the increase of the $Q_{battery}$. The values of m_{min} in the Type I, Type II, Type III, and Type IV are respectively 0.1846kg, 0.3685kg, 0.5514kg, and 0.7351kg when the $Q_{battery}$ is 15W. The m_{min} in the Type I, Type II, Type III, and Type IV are respectively 0.3292kg, 0.6700kg, 0.9958kg, and 1.333kg when the $Q_{battery}$ is 25W. Therefore, the values of m_{min} in the Type I, Type II, Type III, and Type IV are respectively increased by 78.3%, 81.8%, 80.6%, and 81.4%, as the $Q_{battery}$ varies from 15W to 25W.

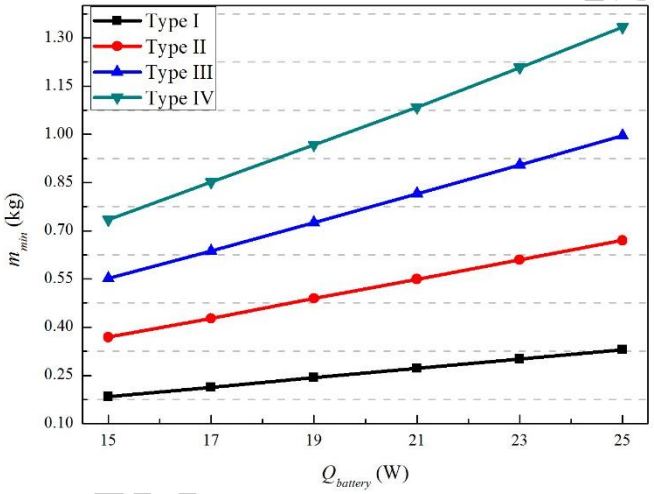

Fig. 15. The variation of the m_{min} with the $Q_{battery}$ for different types of BTMS.

5.5 Comparison between cuboid and cylindrical BTMS

In this part, the $R_{battery}$ and $Q_{battery}$ are set to be 13mm and 15W, respectively. It should be noted that the batteries in the cuboid BTMS have the same configurations with those in the cylindrical BTMS; while the PCM unit in the cuboid BTMS is cuboid. Table 3 shows the comparison of the minimum mass of PCM (m_{min}) between cuboid and cylindrical BTMS for different types of BTMS. The values of m_{min} in the cuboid BMTS are larger than that in the cylindrical BTMS for four types of BTMS. The values of m_{min} in the Type I, Type II, Type III, and Type IV of the cuboid BTMS are respectively 0.1916kg, 0.3733kg, 0.5680kg, and 0.7461kg; while the values of m_{min} in the Type I, Type II, Type III, and Type IV of the cylindrical BTMS are respectively 0.1878kg, 0.3685kg, 0.5514kg, and 0.7351kg.

Table 3 Comparison of the m_{min} values between the cuboid and cylindrical BTMS

	Cuboid BTMS	Cylindrical BTMS
Type I	0.1916 kg	0.1878 kg
Type II	0.3733 kg	0.3685 kg
Type III	0.5680 kg	0.5514 kg
Type IV	0.7461 kg	0.7351 kg

5.6 Effect of top and bottom PCM thickness

In this section the values of PCM thickness (δ_{BTMS}) for the top and bottom of the BTMS are the same. Fig. 16 shows the variation of the (m_{min}) with the δ_{BTMS} for different types of BTMS: (a) Type I; (b) Type II; (c) Type III and (d) Type IV. $R_{battery}$ and $Q_{battery}$ are set to be 13mm and 15W, respectively. It can be observed that the value of m_{min} firstly reduces when the value of δ_{BTMS} increases, and then it increases with the increase of δ_{BTMS} value. Therefore, the optimal values of δ_{BTMS} are 7.5mm, 7.5mm, 5mm and 5mm for Type I, Type II, Type III, and Type IV of BTMS, respectively. In addition, the minimum values of m_{min} are 0.1819kg, 0.3623kg, 0.5461kg, and 0.7309kg for Type I, II, III, and IV of BTMS, respectively.

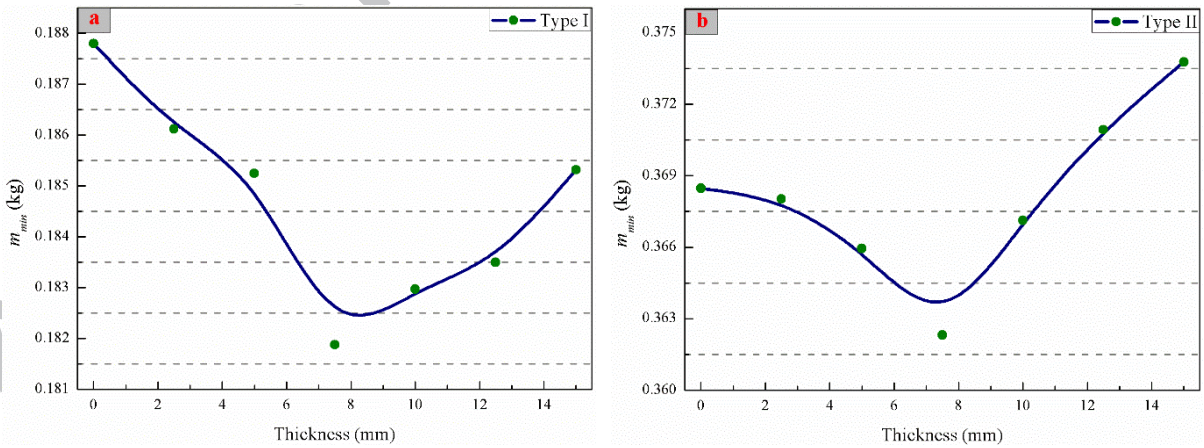

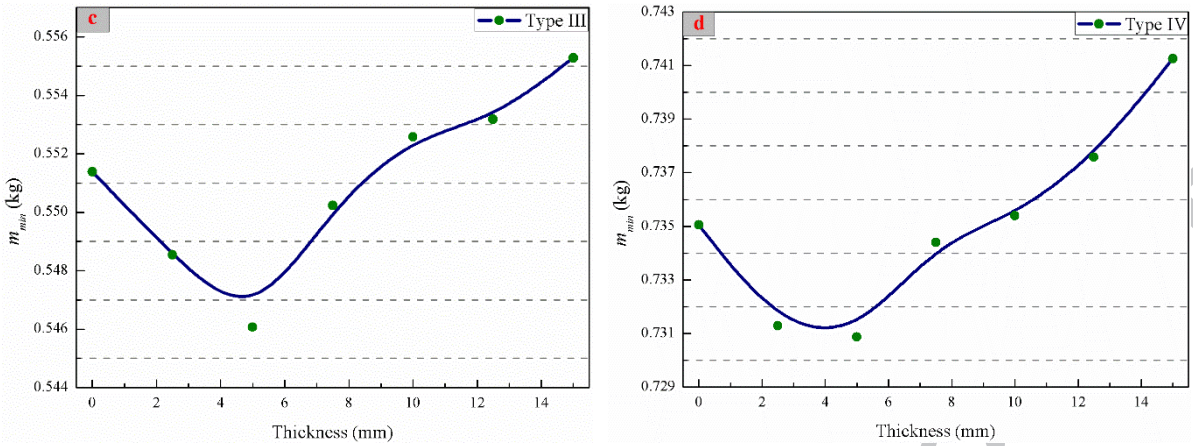

Fig. 16. The variation of the m_{min} with the top and bottom PCM thickness for different types of BTMS.

6. Conclusion

The design optimization method of the BTMS with PCM is proposed in this study. The optimization objective is to minimize the mass of PCM while ensuring two design constraints: (1) the maximum temperature difference in the BTMS should not exceed the threshold value; (2) the desired working time of maintaining the batteries temperature under operation safe temperature should be guaranteed. A case study of the cylindrical BTMS with PCM is presented to illustrate the proposed method. The commercial software CFD is used to solve the thermodynamic equations of the BTMS. To improve the low thermal conductivity of the conventional pure PCM, the EG/PA composite PCM is prepared and utilized in the BTMS. The experimental platform is established to measure the temperature value in the specified locations, and the measurement results are used to validate the numerical solutions. It is found that there is a good agreement between the numerical and experimental results. During the optimization process, four different types of BTMS which respectively use single, double, three and four batteries are considered. The effects of the battery radius, gap between neighboring batteries, heat generation rate, and top and bottom PCM thickness on the minimum mass of PCM are analyzed. In the meantime, the corresponding optimal PCM radiuses are identified in different cases. Therefore, the proposed optimization method can be effectively used to optimize the BTMS with PCM. Moreover, this method provides a meaningful guideline for the manufactures and government to conduct the optimization design of the BTMS with PCM.

Acknowledgement

This work was supported by Guangzhou Science and Technology Program (201704030137) and the Applied Science and Technology Project of Guangdong (2016B020243008).

.

References

[1] M.-D. Yang, M.-D. Lin, Y.-H. Lin, K.-T. Tsai, Multiobjective optimization design of green building envelope material using a non-dominated sorting genetic algorithm, Applied Thermal Engineering, 111 (2017) 1255-1264.

[2] M. Zhang, M. Qin, C. Rode, Z. Chen, Moisture buffering phenomenon and its impact on building energy consumption, Applied Thermal Engineering, 124 (2017) 337-345.

[3] W. Wu, X. Yang, G. Zhang, K. Chen, S. Wang, Experimental investigation on the thermal performance of heat pipe-assisted phase change material based battery thermal management system, Energy Conversion and Management, 138 (2017) 486-492.

[4] Y. Ren, Z. Yu, G. Song, Thermal management of a Li-ion battery pack employing water evaporation, Journal of Power Sources, 360 (2017) 166-171.

[5] A. Greco, X. Jiang, D. Cao, An investigation of lithium-ion battery thermal management using paraffin/porous-graphite-matrix composite, Journal of Power Sources, 278 (2015) 50-68.

[6] Z. Rao, Z. Qian, Y. Kuang, Y. Li, Thermal performance of liquid cooling based thermal management system for cylindrical lithium-ion battery module with variable contact surface, Applied Thermal Engineering, 123 (2017) 1514-1522.

[7] R. Zhao, S. Zhang, J. Liu, J. Gu, A review of thermal performance improving methods of lithium ion battery: Electrode modification and thermal management system, Journal of Power Sources, 299 (2015) 557-577.

[8] G. Jiang, J. Huang, Y. Fu, M. Cao, M. Liu, Thermal optimization of composite phase change material/expanded graphite for Li-ion battery thermal management, Applied Thermal Engineering, 108 (2016) 1119-1125.

[9] N. Javani, I. Dincer, G.F. Naterer, B.S. Yilbas, Heat transfer and thermal management with PCMs in a Li-ion battery cell for electric vehicles, International Journal of Heat and Mass Transfer, 72 (2014) 690-703.

[10] H. Fathabadi, High thermal performance lithium-ion battery pack including hybrid active–passive thermal

management system for using in hybrid/electric vehicles, Energy, 70 (2014) 529-538.

[11] W. Wu, X. Yang, G. Zhang, X. Ke, Z. Wang, W. Situ, X. Li, J. Zhang, An experimental study of thermal management system using copper mesh-enhanced composite phase change materials for power battery pack, Energy, 113 (2016) 909-916.

[12] B. Mortazavi, H. Yang, F. Mohebbi, G. Cuniberti, T. Rabczuk, Graphene or h-BN paraffin composite structures for the thermal management of Li-ion batteries: A multiscale investigation, Applied Energy, 202 (2017) 323-334.

[13] G. Jiang, J. Huang, M. Liu, M. Cao, Experiment and simulation of thermal management for a tube-shell Li-ion battery pack with composite phase change material, Applied Thermal Engineering, 120 (2017) 1-9.

[14] L.H. Saw, Y. Ye, A.A.O. Tay, W.T. Chong, S.H. Kuan, M.C. Yew, Computational fluid dynamic and thermal analysis of Lithium-ion battery pack with air cooling, Applied Energy, 177 (2016) 783-792.

[15] S. Park, D. Jung, Battery cell arrangement and heat transfer fluid effects on the parasitic power consumption and the cell temperature distribution in a hybrid electric vehicle, Journal of Power Sources, 227 (2013) 191-198.

[16] R. Mahamud, C. Park, Reciprocating air flow for Li-ion battery thermal management to improve temperature uniformity, Journal of Power Sources, 196 (2011) 5685-5696.

[17] C.-V. Hémery, F. Pra, J.-F. Robin, P. Marty, Experimental performances of a battery thermal management system using a phase change material, Journal of Power Sources, 270 (2014) 349-358.

[18] A. Jarrett, I.Y. Kim, Design optimization of electric vehicle battery cooling plates for thermal performance, Journal of Power Sources, 196 (2011) 10359-10368.

[19] A. Jarrett, I.Y. Kim, Influence of operating conditions on the optimum design of electric vehicle battery cooling plates, Journal of Power Sources, 245 (2014) 644-655.

[20] L.W. Jin, P.S. Lee, X.X. Kong, Y. Fan, S.K. Chou, Ultra-thin minichannel LCP for EV battery thermal management, Applied Energy, 113 (2014) 1786-1794.

[21] M.-S. Wu, K. Liu, Y.-Y. Wang, C.-C. Wan, Heat dissipation design for lithium-ion batteries, Journal of Power Sources, 109 (2002) 160-166.

[22] Z. Rao, S. Wang, M. Wu, Z. Lin, F. Li, Experimental investigation on thermal management of electric vehicle battery with heat pipe, Energy Conversion and Management, 65 (2013) 92-97.

[23] A. de Gracia, E. Oró, M.M. Farid, L.F. Cabeza, Thermal analysis of including phase change material in a domestic hot water cylinder, Applied Thermal Engineering, 31 (2011) 3938-3945.

[24] L.F. Cabeza, H. Mehling, S. Hiebler, F. Ziegler, Heat transfer enhancement in water when used as PCM in thermal energy storage, Applied Thermal Engineering, 22 (2002) 1141-1151.

[25] Y. Li, G. Huang, T. Xu, X. Liu, H. Wu, Optimal design of PCM thermal storage tank and its application for winter available open-air swimming pool, Applied Energy, 209 (2018) 224-235.

[26] W.G. Alshaer, S.A. Nada, M.A. Rady, C. Le Bot, E. Palomo Del Barrio, Numerical investigations of using carbon foam/PCM/Nano carbon tubes composites in thermal management of electronic equipment, Energy Conversion and Management, 89 (2015) 873-884.

[27] S.A. Nada, W.G. Alshaer, Comprehensive parametric study of using carbon foam structures saturated with PCMs in thermal management of electronic systems, Energy Conversion and Management, 105 (2015) 93-102.

[28] Y. Huo, Z. Rao, Investigation of phase change material based battery thermal management at cold temperature using lattice Boltzmann method, Energy Conversion and Management, 133 (2017) 204-215.

[29] R. Liu, J. Chen, J. Xun, K. Jiao, Q. Du, Numerical investigation of thermal behaviors in lithium-ion battery stack discharge, Applied Energy, 132 (2014) 288-297.

[30] F. Samimi, A. Babapoor, M. Azizi, G. Karimi, Thermal management analysis of a Li-ion battery cell using phase change material loaded with carbon fibers, Energy, 96 (2016) 355-371.

[31] K. Somasundaram, E. Birgersson, A.S. Mujumdar, Thermal–electrochemical model for passive thermal management of a spiral-wound lithium-ion battery, Journal of Power Sources, 203 (2012) 84-96.

[32] W.Q. Li, Z.G. Qu, Y.L. He, Y.B. Tao, Experimental study of a passive thermal management system for high-powered lithium ion batteries using porous metal foam saturated with phase change materials, Journal of Power Sources, 255 (2014) 9-15.

[33] C. Lin, S. Xu, G. Chang, J. Liu, Experiment and simulation of a LiFePO4 battery pack with a passive thermal management system using composite phase change material and graphite sheets, Journal of Power Sources, 275 (2015) 742-749.

[34] A.P. Sasmito, T. Shamim, A.S. Mujumdar, Passive thermal management for PEM fuel cell stack under cold weather condition using phase change materials (PCM), Applied Thermal Engineering, 58 (2013) 615-625.

[35] F. Bruno, N.H.S. Tay, M. Belusko, Minimising energy usage for domestic cooling with off-peak PCM storage, Energy and Buildings, 76 (2014) 347-353.

[36] N.A.M. Amin, M. Belusko, F. Bruno, M. Liu, Optimising PCM thermal storage systems for maximum energy storage effectiveness, Solar Energy, 86 (2012) 2263-2272.

[37] Z. Ling, J. Chen, X. Fang, Z. Zhang, T. Xu, X. Gao, S. Wang, Experimental and numerical investigation of

the application of phase change materials in a simulative power batteries thermal management system, Applied Energy, 121 (2014) 104-113.

[38] I. ANSYS, CFD tutorial manual, Release 14.5, Accessed on 30 October 2012, in.

[39] A. Fluent, 13.0 Theory Guide, Turbulence, ANSYS Inc., Canonsburg, PA, (2010).

[40] A. Väyrynen, J. Salminen, Lithium ion battery production, The Journal of Chemical Thermodynamics, 46 (2012) 80-85.

[41] A. Babapoor, M. Azizi, G. Karimi, Thermal management of a Li-ion battery using carbon fiber-PCM composites, Applied Thermal Engineering, 82 (2015) 281-290.

[42] Z. Ling, J. Chen, T. Xu, X. Fang, X. Gao, Z. Zhang, Thermal conductivity of an organic phase change material/expanded graphite composite across the phase change temperature range and a novel thermal conductivity model, Energy Conversion and Management, 102 (2015) 202-208.

[43] Z. Ling, F. Wang, X. Fang, X. Gao, Z. Zhang, A hybrid thermal management system for lithium ion batteries combining phase change materials with forced-air cooling, Applied Energy, 148 (2015) 403-409.

Highlights

- An optimization method for minimizing PCM mass in the Li-ion thermal management system is proposed.
- This method is applied in a typical cylindrical thermal management system with PCM.
- Effects of different geometrical parameters on the optimal PCM mass are investigated.
- The developed method can effectively optimize the PCM mass in the thermal management system